Single-wall carbon nanotubes phonon spectra: Symmetry-based calculations

E. Dobardžić,* I. Milošević, B. Nikolić, T. Vuković, and M. Damnjanović
Faculty of Physics, University of Belgrade, P.O. Box 368, 11001 Belgrade, Serbia, Yugoslavia
(Received 21 December 2002; revised manuscript received 10 March 2003; published 10 July 2003)

The phonon dispersions and atomic displacements for single-wall carbon nanotubes of arbitrary chirality are calculated. The full symmetry is implemented. The approach is based on the force constants of graphene, with the symmetry imposed modifications providing the twisting acoustic mode exactly. The functional dependence of frequencies of the Raman and infrared active modes on the wrapping angle and on the diameter are presented. The armchair tubes are found to be infrared inactive under the light linearly polarized along the tube axis. Also the overbending absolute value and the wave vector dependence on the tube geometry are found and the chirality selective method for the sample characterization is proposed. Finally, the specific heat calculations are carried out.

DOI: 10.1103/PhysRevB.68.045408 PACS number(s): 61.46.+w, 63.22.+m, 65.80.+n

I. INTRODUCTION

Elastic and vibrational properties of the single-wall carbon nanotubes (SWCNTs)[1] have been studied extensively by many research groups[2] and a large variety of the methods have been applied: simple and modified zone folding,[3,4] nonorthogonal[5] and orthogonal tight-binding Hamiltonian models fitted to the graphite,[6] force constant[7] and valence force field[8] model, effective potential,[9] and *ab initio*[10] calculations. Recently, *ab initio* calculations (with comparison to other methods) for some SWCNTs have been reported.[11] In this paper we present the results of the symmetry-based method of the SWCNT's phonon dispersion calculations. By using the full symmetry group of the SWCNT's (Ref. 12) we easily carry out numerical evaluations of the phonon spectra for the tubes of any chiralities and diameters. Also, we solved exactly the problem of adjusting the graphene force constants to the SWCNT geometry, and get the rotational acoustic mode.

Our preliminary results on the SWCNT's phonon dispersions have already been highlighted within the Raman scattering framework.[13] In this paper we present detailed description of the method we are applying and present complete, thoroughly tested, results on the vibrational properties of the SWCNT's. This group theoretical concept enables also calculation of the dispersions of multiwall carbon nanotubes: the spectra of the double-wall ones we expect to report soon.

We adopt the model of ideally structured infinite and isolated SWCNT (Ref.12) and apply the line group.[14]theoretical approach: the modified Wigner projectors procedure[15,16] implemented into the computer program POLSym.[17] This improves both the precision and efficiency of the calculations, enabling us to study the phonon dispersions and corresponding eigenvectors for 1280 SWCNT's (all the tubes with diameters in the interval [2.8 Å, 50.0 Å]). It is reliable statistics for the investigations of the dependence of the various phonon spectra properties on the parameters such as the tube helicity and diameter. Apart from the technical advantages, the full symmetry implementation gives many fundamental results: the phonon bands assignment by the full set of the conserved quantum numbers, band degeneracy, and the selection rules for various processes,[18] extraction of the Raman and infrared (IR) active modes.

In what follows we firstly introduce the computational method and explain briefly its specific symmetry-based core, which is not incorporated in the other force-constant methods (Sec. II). Then we give the results that stem from the line group symmetry considerations only and the Raman and IR active-modes frequencies as functions of the tube parameters (Sec. III). In Sec. IV we discuss the phonon dispersions, laser excitation energy dependence of the high-frequency Raman active mode and related to that, the overbending wave vector and chiral angle dependence, the heat capacity, sound velocities, and some other details. The paper ends with the brief summary (Sec. V).

II. METHOD

A. Computational scheme

The computational code POLSym, which we use in this study, was originally applied to the DNA molecule and presented *in extenso* elsewhere.[17] It is based on the modified Wigner projectors for induced representations[15]and line group symmetry.[14]

We consider an infinitely long, isolated, and perfectly structured SWCNT, impose no periodic boundary conditions on its geometry and take a benefit of the fact that a SWCNT is a single-orbit system (i.e., the cylindrical carbon web can be obtained from any atom by action of the symmetry group of the tube considered). This way we maximally reduce the dimension of the eigenvalue problem to be solved, to at most 12. In principle, this dimension is the product of the following three factors: (i) number of the orbits of the system (1 for SWCNT's), (ii) dimension of the orbit representative interior space (3 for phonons), and (iii) dimension of the relevant irreducible representation (1 or 2 for the chiral; 1, 2, or 4 for the achiral SWCNT's). Each irreducible representation, i.e., each set of quantum numbers, defines the so-called transfer operators,[15] which pull down the eigen problem to such a low-dimensional space. The dispersions are automatically obtained as the eigenvalues of the reduced (pulled-down) operators. To get the displacements, the eigenvector of this pulled-down problem is mapped back to the entire space and

the partial (over the irreducible space only) scalar product taken. Full mathematical formalism of the tight-binding method (being applicable to molecular dynamics calculations as well) we use in this work is presented in Ref. 16 and references therein.

B. Symmetry

Line groups[14] (known also as rod or monoperiodic groups) are the maximal subgroups of the Euclidean group that leave the quasi-one-dimensional crystals invariant. Symmetry groups of chiral (n_1,n_2), zig-zag $(n,0)$, and armchair (n,n) tubes ($\mathcal{C}$, $\mathcal{Z}$, and $\mathcal{A}$, for short) are nonsymmorphic line groups:[12] $\boldsymbol{L}_{\mathcal{C}}=\boldsymbol{T}_q^r\boldsymbol{D}_n=\boldsymbol{L}q_p22$, $\boldsymbol{L}_{\mathcal{ZA}}=\boldsymbol{T}_{2n}^1\boldsymbol{D}_{nh}=\boldsymbol{L}2n_n/mcm$. Here, n is the greatest common divisor of n_1 and n_2, $q=2(n_1^2+n_1n_2+n_2^2)/n\mathcal{R}$ is the order of the isogonal group principle axis, $\mathcal{R}=3$ if $(n_1-n_2)/3n$ is integer, otherwise $\mathcal{R}=1$, while the parameters r and p describe the helicity by more complicated functions[12] of n_1 and n_2. The general line group element is $\ell_{tsuv}=(C_q^r|na/q)^tC_n^sU^u\sigma_{\mathrm{v}}^v$, where C_n^s $(s=0,\ldots,n-1)$ is the rotation through $2\pi s/n$ around the tube axis (z axis), the Koster-Seitz symbol $(C_q^r|na/q)^t$ $(t=0,\pm1,\ldots;$ a is the translational period of the tube) denotes the rotation for $2rt\pi/q$ around the tube axis followed by the translation along it for nat/q, while U is the rotation through π (thus $u=0,1$) around the horizontal axis through the center of a carbon hexagon perpendicularly to the tube. We fix a tube reference frame[12] so that x and z axes coincide with the U and the tube axes, respectively. Achiral tubes have an extra symmetry: vertical mirror reflection σ_{v} in the xz plane (for $\mathcal{C}$ tubes one should take $v=0$). Note that, having both σ_{v} and U symmetry, $\mathcal{Z}$ and $\mathcal{A}$ tubes have horizontal (xy) mirror plane symmetry $\sigma_{\mathrm{h}}=\sigma_{\mathrm{v}}U=U\sigma_{\mathrm{v}}$ as well. By mapping any carbon atom by the entire set of the transformations $\ell_{tsu}=\ell_{tsu0}$ [which are concretely defined by the wrapping indices (n_1,n_2)] one builds the corresponding tube. In other words, SWCNT is a single-orbit system and its carbon atoms can be labeled as C_{tsu}.

The symmetry singles out the complete set of the quantum numbers of quasimomenta and parities. The pair of the z components of linear and total angular quasimomenta k and m is most frequently used, although m is not conserved. While k runs over the Brillouin zone (BZ) $(-\pi/a,\pi/a]$, m takes on the integer values from $(-q/2,q/2]$ (note that q is even). Besides the quasimomenta, there is a parity with respect to the twofold horizontal axis, and for the achiral tubes only, in addition, there are vertical and horizontal mirror parities.

Each normal mode is assigned by a set μ of these quantum numbers (i.e., μ is a particular choice of k, m, and the parities values). The same set singles out the irreducible representation D^{μ} (i.e., $|\mu|$-dimensional matrices[16] explicating the law of the mode transformations under the symmetries). Let $\boldsymbol{e}^{\mu M}=\{\ldots,\boldsymbol{e}^{\mu M}(\alpha),\ldots\}$ denotes such a mode, in accordance with the usual notation:[19] the atom α is displaced by the vector $\boldsymbol{e}^{\mu M}(\alpha)$ with the coordinates $\boldsymbol{e}_i^{\mu M}(\alpha)$. Note that $M=1,\ldots,|\mu|$ distinguishes between the degenerate modes forming the multiplet of D^{μ}. Then the transformations ℓ_{tsuv} mix the modes only within the same multiplet:

$$\ell_{tsuv}\boldsymbol{e}^{\mu M}=\sum_{M'}D^{\mu}_{M'M}(\ell_{tsuv})\boldsymbol{e}^{\mu M'}.$$

Each mode $\boldsymbol{e}^{\mu M}$ is a collective vibration of the SWCNT atoms, i.e., it consists of the three-dimensional (3D) displacements $\boldsymbol{e}^{\mu M}(tsu)$ of all the C_{tsu} atoms. Within the full symmetry implemented tight-binding method,[16] the modified group projectors technique uses the symmetry to transfer the relevant information to the three-dimensional configuration space of initial atom C_{000} (multiplied by the space of the considered irreducible representation). The results of the eigenvalue problem are the normal mode frequencies and the displacements $\boldsymbol{e}^{\mu M}(000)$ of this atom. Finally, the same technique employs symmetry to determine the displacements of other atoms from $\boldsymbol{e}^{\mu M}(000)$ in the generalized Bloch form,[15] which for SWCNT (being a single-orbit system) reduces to

$$\boldsymbol{e}^{\mu M}(tsu)=\sum_{M'}D^{\mu}_{M'M}(\ell_{tsu})D^{\mathrm{pv}}(\ell_{tsu})\boldsymbol{e}^{\mu M'}(000), \quad (1)$$

where D^{pv} denotes the vector representation of the symmetry group.

Working with the space of initial atom C_{000} only, the modified group projectors technique[15,16] establishes the generalized Bloch form of the normal mode: conveniently, as for any single-orbit system, all the atomic displacements are determined by that of the C_{000} atom.

C. Force-constant model

We start with the graphite force constants,[3] and adjust them (kinematically and dynamically) to the nanotube geometry. To clarify this two-step modification, in the dynamical matrix[19] we single out the 3×3 submatrix Φ_{β}^{α} with elements $\Phi_{\beta j}^{\alpha i}=\Phi_{ij}(\alpha,\beta)$, referring to the pair (α,β) of carbon atoms. For the atoms α and β, the stretching direction is along the unit vector $|\alpha\beta,1\rangle$ from α to β, the out-of-plane unit vector $|\alpha\beta,2\rangle$ is perpendicular both to the tube axis and to $|\alpha\beta,1\rangle$, while the in-plane unit vector is $|\alpha\beta,3\rangle=|\alpha\beta,1\rangle\times|\alpha\beta,2\rangle$. These three vectors are assumed to be the eigenvectors of the matrix Φ_{β}^{α}, with the force constants $c_i^{\alpha\beta}$ as the corresponding eigenvalues: $\Phi_{\beta}^{\alpha}|\alpha\beta,i\rangle=c_i^{\alpha\beta}|\alpha\beta,i\rangle$. With the help of the eigenvectors' coordinates in the tube's reference frame $|\alpha\beta,i\rangle=(S_{1i}^{\alpha\beta},S_{2i}^{\alpha\beta},S_{3i}^{\alpha\beta})$, the coordinate form of the extracted submatrix is found: $\Phi_{\beta}^{\alpha}=\Sigma_i c_i^{\alpha\beta}|\alpha\beta,i\rangle\langle\alpha\beta,i|$, i.e., $\Phi_{\beta j}^{\alpha i}=\Sigma_p c_p^{\alpha\beta}S_{ip}^{\alpha\beta}S_{jp}^{\alpha\beta}$.

As the first step, we make pure kinematic modification that provides the twisting mode exactly. Recall the rotational sum rule:[20]

$$\sum_{\beta}(R_{\alpha\beta1}\Phi_{\beta2}^{\alpha j}-R_{\alpha\beta2}\Phi_{\beta1}^{\alpha j})=0, \quad \forall\alpha, \quad j=1,2,3 \quad (2)$$

where the sum runs over the relevant neighbors β of the atom α $(\beta\neq\alpha)$, $\Phi_{\beta i}^{\alpha j}$ is an element of the matrix Φ_{β}^{α}, and $R_{\alpha\beta i}$ is the Cartesian component of the vector $\boldsymbol{R}_{\alpha\beta}$ from α to β in the equilibrium positions (note that $|\alpha\beta,1\rangle$

$=\boldsymbol{R}_{\alpha\beta}/R_{\alpha\beta}$). As $|\alpha\beta,2\rangle$ is orthogonal to the tube axis, its z component $S_{32}^{\alpha\beta}$ vanishes. Thus, coordinate form of Eq. (2) reduces to

$$\sum_{\beta} R_{\alpha\beta}(c_2^{\alpha\beta}S_{j2}^{\alpha\beta}S_{33}^{\alpha\beta}-c_3^{\alpha\beta}S_{j3}^{\alpha\beta}S_{32}^{\alpha\beta})=0, \quad j=1,2,3,\forall\,\alpha,$$

i.e., to the pair of equations for each α atom,

$$\sum_{\beta} R_{\alpha\beta}c_2^{\alpha\beta}S_{12}^{\alpha\beta}S_{33}^{\alpha\beta}=0, \quad \sum_{\beta} R_{\alpha\beta}c_2^{\alpha\beta}S_{22}^{\alpha\beta}S_{33}^{\alpha\beta}=0. \quad (3)$$

Note that these conditions involve the out-of-plane force constants only. As has already been emphasized a SWCNT is a single-orbit system, which enables to perform the calculations (within the modified group projector technique) by considering one carbon atom only, e.g., the orbit representative $\alpha=\mathrm{C}_{000}$. Thus, Eq. (3) imposes two conditions altogether. These are included exactly as follows. Up to the fourth level there are 18 neighbors; collecting all the out-of-plane force constants in the vector $c_2^{\alpha}=(c_2^{\alpha 1},\ldots,c_2^{\alpha 18})$, Eq. (3) gives the orthogonality conditions $c_2^{\alpha}\cdot S_j^{\alpha}=0$, $j=1,2$, where the vectors $S_k^{\alpha}=(R_{\alpha 1}S_{k2}^{\alpha 1}S_{33}^{\alpha 1},\ldots,R_{\alpha 18}S_{k2}^{\alpha 18}S_{33}^{\alpha 18})$ comprise the coordinate factors. Thus, any choice of the force constants producing the vector c_2^{α} simultaneously orthogonal to the vectors S_1^{α} and S_2^{α} will exactly provide the twisting acoustic mode. It is, therefore, natural to correct the physically suitable set of the graphene force constants minimally, projecting them out onto the orthocomplement of the plane defined by S_1^{α} and S_2^{α}.

In order to include the dynamical response to the configuration changes (due to the rolling up of a graphene plane) we make Ansatz that is analogous to that presented in the work of Saito *et al.*[4] In the frame in which z axis coincides with the tube axis and x axis runs through the atom α, the eigenbasis of Φ_{β}^{α} reads

$$|\alpha\beta,1\rangle=\left(-\cos\psi\sin\frac{\varphi}{2},\cos\psi\cos\frac{\varphi}{2},\sin\psi\right),$$

$$|\alpha\beta,2\rangle=\left(\cos\frac{\varphi}{2},\sin\frac{\varphi}{2},0\right), \quad (4)$$

$$|\alpha\beta,3\rangle=\left(-\sin\psi\sin\frac{\varphi}{2},\sin\psi\cos\frac{\varphi}{2},-\cos\psi\right).$$

Here, φ is a cylindrical coordinate of the β atom and ψ is the angle between the horizontal xy plane and the straight line that connects α and β. On the other hand, the graphene stretching, out-of-plane and in-plane unit vectors $|\alpha_g\beta_g,i\rangle$ are in the SWCNT's geometry obtained by rolling up a graphene sheet: $|\alpha_g\beta_g,1\rangle$ becomes the tangent to the projection of the line connecting α and β to the tube's surface, $|\alpha_g\beta_g,2\rangle$ is perpendicular to the tube at α, while again $|\alpha_g\beta_g,3\rangle=|\alpha_g\beta_g,1\rangle\times|\alpha_g\beta_g,2\rangle$. Their coordinates, in the same reference frame as Eq. (4), are the following:

$$|\alpha_g\beta_g,1\rangle=\left(0,\frac{\cos\frac{\varphi}{2}\cos\psi}{\sqrt{1-\sin^2\frac{\varphi}{2}\cos^2\psi}},\frac{\sin\psi}{\sqrt{1-\sin^2\frac{\varphi}{2}\cos^2\psi}}\right),$$

$$|\alpha_g\beta_g,2\rangle=(1,0,0), \quad (5)$$

$$|\alpha_g\beta_g,3\rangle=\left(0,\frac{\sin\psi}{\sqrt{1-\sin^2\frac{\varphi}{2}\cos^2\psi}},-\frac{\cos\frac{\varphi}{2}\cos\psi}{\sqrt{1-\sin^2\frac{\varphi}{2}\cos^2\psi}}\right).$$

The Ansatz is to modify the original graphene force constants $C_i^{\alpha_g\beta_g}$ so to provide that the component of the ith force ($i=1,2,3$) along $|\alpha_g\beta_g,i\rangle$ is of the same intensity as in the graphene plane. Simple geometry shows the required modified constants $c_i^{\alpha\beta}$ to be related to the original ones *via* $c_i^{\alpha\beta}=C_i^{\alpha_g\beta_g}/|\langle\alpha_g\beta_g,i|\alpha\beta,i\rangle|$. The expansion over sine and cosine of $\varphi/2$ yields

$$c_1^{\alpha\beta}=C_1^{\alpha_g\beta_g}\left(2-\cos\frac{\varphi}{2}\right),$$

$$c_2^{\alpha\beta}=C_2^{\alpha_g\beta_g}\left[1+\sin^2\psi\left(1-\cos\frac{\varphi}{2}\right)\right], \quad (6)$$

$$c_3^{\alpha\beta}=C_3^{\alpha_g\beta_g}\left[1+\cos^2\psi\left(1-\cos\frac{\varphi}{2}\right)\right].$$

In our calculations we first find the dynamically corrected graphene force constants by Eqs. (6), and afterward project them. It should be noted that the kinematical correction is dominant, in the sense that if it is applied directly to the graphene constants, avoiding the dynamical correction, the results differ only slightly, except for the very thin tubes. In general, due to the similar dynamical correction introduced, our results are close to that of Ref. 4, with exactly four acoustic mode.

III. ACOUSTIC, RAMAN, AND IR ACTIVE MODES

The quantum numbers of the momentum component p_z (along the tube axis; tensor ${}_0A_0^-$) are $k=0$ and $m=0$. As for the parities, it changes the sign upon the z reversal transformations and is invariant under the vertical mirror reflections. Concerning the transversal momenta components, they span the 2D irreducible subspace of the ${}_0E_1^{(+)}$ tensor; thus, $k=0$, $m=\pm 1$, and for the achiral tubes only (therefore in the brackets) $+$ for the horizontal mirror invariance. Hence, the polar vectors, such as the linear momentum, transform according to the representation D^{pv} decomposing as ${}_0A_0^- + {}_0E_1^{(+)}$. This further means that besides $k=0$ for all the acoustic modes, for the longitudinal translation m vanishes as well, while the two lateral translations are degenerate and characterized by $m=\pm 1$. Naturally, longitudinal translation

changes sign upon the z reversal and is not affected by the vertical mirror, while the lateral ones, due to their degeneracy, have no defined parity besides the horizontal mirror invariance. The twisting mode is, with $m=0$, odd with respect to the σ_v and U transformations and, consequently, invariant under the horizontal mirror reflections (tensor ${}_0A_0^-$ for chiral and ${}_0B_0^+$ for achiral SWCNT's). Bearing this in mind, it is easy to extract the IR and Raman active modes from the SWCNT's dynamical representations.[12]

The linear momentum quantum numbers determine the IR active modes as well: in the dipole approximation the incident electric field polarized parallel to the tube axis involves p_z; perpendicular linear polarization relates p_x and p_y, while the standard components $p_\pm=(p_x \mp i\, p_y)/2$ describe the circular polarization. For the chiral tubes we find six IR active modes, out of which only one (of the ${}_0A_0^-$ type) is active under the parallel and all the others (${}_0E_1$) under the perpendicular (either linear or circular) polarization of the light. It should be stressed out that in the armchair configuration, there are no active modes for the parallel polarization, unlike the zig-zag case where there is one such mode. Under perpendicularly (or xy circularly) polarized light, there are three (two) active modes in the armchair (zig-zag) configuration.

The momenta quantum numbers further determine the selection rules for first-order Raman scattering. The total Raman tensor transforms as the square $D^{\mathrm{pv}}\otimes D^{\mathrm{pv}}$ of the vector representation. Its symmetric and antisymmetric parts correspond to the symmetrized and antisymmetrized squares: $[D^{\mathrm{pv}}]^2=2_0A_0^+ + {}_0E_1 + {}_0E_2$ and $\{D^{\mathrm{pv}}\}^2={}_0A_0^- + {}_0E_1$ for the chiral SWCNT's, while in the achiral cases $[D^{\mathrm{pv}}]^2=2_0A_0^+ + {}_0E_1^- + {}_0E_2^+$ and $\{D^{\mathrm{pv}}\}^2={}_0B_0^+ + {}_0E_1^-$. The antisymmetric part of the Raman tensor should be relevant generally for the chiral systems,[21] as well as in the resonant scattering processes, which proved to be important in SWCNT's.

By the use of the above decomposition, we extract the IR and Raman active modes from the SWCNT's dynamical representations.[12] As for the symmetric part of Raman tensor, in accordance with Ref. 22, for the chiral tubes we find 14 active modes: $3_0A_0^+$, 5_0E_1, and 6_0E_2. The achiral tubes have eight Raman active modes out of which two are totally symmetric. The other six phonon modes are of the types ${}_0E_1^-$ and ${}_0E_2^+$ (three of each for the zig-zag and two and four, respectively, for the armchair tubes).

When both the incoming and outgoing light are polarized along the tube axis, the electron transitions occur between the subbands with the same quantum numbers, and only $m=0$ phonons accompany such processes. At $k=0$ these are totally symmetric modes ${}_0A_0^+$: besides the low-frequency radial-breathing mode (RBM), for the chiral tubes there are two such high-frequency modes (HFM). Nevertheless, being odd in the vertical mirror parity, one of the HFM's (second/third in Table I) becomes Raman inactive in the case of the zig-zag/armchair tubes; the remaining one is with out-of-phase displacements orthogonal/tangential to the tube circumference. In the case of the crossed polarization, the phonon mode required is of the ${}_0E_1^{(-)}$ type (i.e. with $m=\pm 1$), while when both the incoming and outgoing light are polarized perpendicularly to the tube axis, the phonons in the Raman process should satisfy $m=0$ or $m=\pm 2$. They are either totally symmetric (as in the parallel-parallel case) or of the ${}_0E_2^+$ type, since the electron can be scattered from $m-1$ to $m+1$ subband. As well as the symmetric one, the antisymmetric scattering with the crossed polarization is in all the tubes enabled by the mode ${}_0E_1^{(-)}$. The antisymmetric scattering with both incoming and the scattered light polarized perpendicularly is allowed in chiral and armchair tubes only, due to the extra (besides the twisting acoustic) ${}_0A_0^-$, i.e., ${}_0B_0^+$ mode; this is related to the $\Delta m=0$ electronic transitions. The scattering with parallel polarization of the incoming and scattered light is totally symmetric for all the tube types; in the zig-zag tubes such is also the scattering with both polarizations being orthogonal.

The diameter dependence of the Raman active-mode frequencies we give in Table I. The fit is made over 1280 SWCNT's in the diameter range [2.8 Å , 50.0 Å], which incorporates all the tubes between (2,2) and (53,18), in particular, the zig-zag tubes from (4,0) to (63,0) and the armchair from (2,2) to (36,36). In Fig. 1 (right panel) we give, for the tube (15,4), the dispersions of the branches that, at $k=0$, end up by the Raman and IR active modes.

The first entry in Table I is the RBM. However, it has z component except in the armchair case. Otherwise, it shows a nonvanishing component along the tube axis that depends on the chiral angle θ and decreases with the diameter D. For the unit outward displacement, the longitudinal component of the RBM is well fitted by

$$z_{\mathrm{RBM}}(D,\theta)=\left(\frac{0.197}{D}-\frac{0.167}{D^3}\right)\cos 3\theta \qquad (7)$$

(D should be inserted in angstroms). Indeed, in the armchair tubes, as all the atoms lay in one (of infinitely many) horizontal mirror plane, the symmetric modes (denoted by superscript $+$) must have vanishing longitudinal component. In contrast, for the σ_h-odd modes ($-$) the horizontal component necessarily disappears. As all the $k=0$ modes are either even or odd in σ_h, they are either perpendicular or parallel to the tube axis. Analogously, the atoms in the zig-zag tubes lay in the vertical mirror planes and the symmetric (A) atomic displacements are necessarily within these planes, while the σ_v-antisymmetric ones (B) are tangential to the tube circumference. This refers to the entire subbands with $m=0,n$, since unlike the σ_h which characterizes only $k=0$ states for all m, the vertical mirror parity is defined for all k but for $m=0,n$ only.

IV. PHONON DISPERSION CURVES

A. General characteristics

The number of the carbon atoms per unit cell of the nanotube is $N=2q$, giving for the chiral tubes $6q$ double degenerate phonon branches over $k\in[0,\pi/a]$. Four of them are acoustic. In the achiral cases $q=2n$ and there are 12 double and $6(n-1)$ four-fold degenerate branches. The angular momentum quantum numbers of the former are $m=0,n$, while

TABLE I. Frequencies of the Raman and IR active modes as functions of the tube diameter D and the chiral angle θ. The classification is based on the irreducible representations of the chiral tubes (first column). In the second and third column the corresponding representations of the zig-zag and armchair tubes are given. For each type of SWCNT's, all the processes in which the mode is active are indicated: *I* and *R* stand for IR and Raman activity, respectively, with the polarization of incident and scattered light indicated in the superscript; $[R]$ and $\{R\}$ emphasize that the mode contributes to the symmetric and antisymmetric part only of the Raman tensor. In the last column we give the fitted functional dependence $\omega(D,\theta)$ (ω in cm^{-1} for D in Å). Obviously, the first term in the expansion is the limiting graphene value. Apart from this, for the tubes (12,8), (17,0), and (10,10) the concrete values of the IR and Raman active-mode frequencies are listed in the first three columns, respectively.

Chiral		(12,8)	Zig-zag		(17,0)	Armchair		(10,10)	$\omega(D,\theta)$
${}_0A_0^+$	$[R]^{\parallel\parallel},[R]^{\perp\perp}$	164	${}_0A_0^+$	$[R]^{\parallel\parallel},[R]^{\perp\perp}$	168	${}_0A_0^+$	$[R]^{\parallel\parallel},[R]^{\perp\perp}$	165	$0+\frac{2243}{D}-\frac{665}{D^3}$
		1584	${}_0B_0^-$	—	1584	${}_0A_0^+$	$[R]^{\parallel\parallel},[R]^{\perp\perp}$	1584	$1588-\frac{757.6\cos\theta}{D^2}-\frac{1069.9\cos\theta}{D^4}$
		1587	${}_0A_0^+$	$[R]^{\parallel\parallel},[R]^{\perp\perp}$	1588	${}_0B_0^-$	—	1588	$1588+\frac{59.8\cos 6\theta}{D^2}$
${}_0A_0^-$	$\{R\}^{\perp\perp},I^{\parallel}$	873	${}_0A_0^-$	$I^{\parallel}$	873	${}_0B_0^+$	$\{R\}^{\perp\perp}$	873	$868+\frac{1450}{D^2}-\frac{3899.4}{D^4}$
${}_0E_1$	$R^{\parallel\perp},R^{\perp\parallel},I^{\perp}$	116	${}_0E_1^-$	$R^{\parallel\perp},R^{\perp\parallel}$	119	${}_0E_1^-$	$R^{\parallel\perp},R^{\perp\parallel}$	117	$0+\frac{1588.6}{D}-\frac{5180.8\cos 2\theta}{D^4}$
		232	${}_0E_1^+$	$I^{\perp}$	238	${}_0E_1^+$	$I^{\perp}$	233	$0+\frac{3157.7}{D}-\frac{139426\sin\left(\frac{\pi}{3}+2\theta\right)}{D^6}$
		871	${}_0E_1^-$	$R^{\parallel\perp},R^{\perp\parallel}$	871	${}_0E_1^+$	$I^{\perp}$	871	$865+\frac{1510.7\cos\frac{\theta}{2}}{D^2}-\frac{5073.1\cos\left(\frac{\pi}{12}+\theta\right)}{D^3}$
		1583	${}_0E_1^-$	$R^{\parallel\perp},R^{\perp\parallel}$	1585	${}_0E_1^+$	$I^{\perp}$	1586	$1588-\frac{1037.6\cos\left(\frac{\pi}{3}-\theta\right)}{D^2}-\frac{3311.6\cos^2\left(\frac{\pi+9\theta}{6}\right)}{D^3}$
		1586	${}_0E_1^+$	$I^{\perp}$	1584	${}_0E_1^-$	$R^{\parallel\perp},R^{\perp\parallel}$	1583	$1588+\frac{48.8\cos^2\left(\frac{\pi}{6}-\theta\right)}{D}-\frac{967.3\cos^2\left(\frac{\pi-6\theta}{12}\right)}{D^2}$
${}_0E_2$	$[R]^{\perp\perp}$	21	${}_0E_2^+$	$[R]^{\perp\perp}$	21	${}_0E_2^+$	$[R]^{\perp\perp}$	21	$0+\frac{4254.7}{D^2}-\frac{5556.4}{D^3}$
		231	${}_0E_2^-$	—	236	${}_0E_2^-$	—	233	$0+\frac{3190.9}{D}-12121.5\cos\left(\frac{\pi}{6}+\theta\right)D^3$
		365	${}_0E_2^+$	$[R]^{\perp\perp}$	376	${}_0E_2^+$	$[R]^{\perp\perp}$	367	$0+\frac{5012.8}{D}-\frac{74799.2\cos\left(\frac{\pi}{3}-\theta\right)}{D^4}$
		865	${}_0E_2^-$	—	865	${}_0E_2^+$	$[R]^{\perp\perp}$	866	$865+\frac{860.3}{D^2}-\frac{10196.6\cos\theta}{D^3}$
		1570	${}_0E_2^+$	$[R]^{\perp\perp}$	1570	${}_0E_2^-$	—	1569	$1588-\frac{3891.2}{D^2}+\frac{8395.2\cos\left(\frac{\pi}{6}+\theta\right)}{D^3}$
		1589	${}_0E_2^-$	—	1587	${}_0E_2^+$	$[R]^{\perp\perp}$	1589	$1588+\frac{753.3\cos^2\left(\frac{\pi+6\theta}{12}\right)}{D^2}-\frac{14731.2\cos\left(\frac{\pi}{6}+\theta\right)}{D^3}$

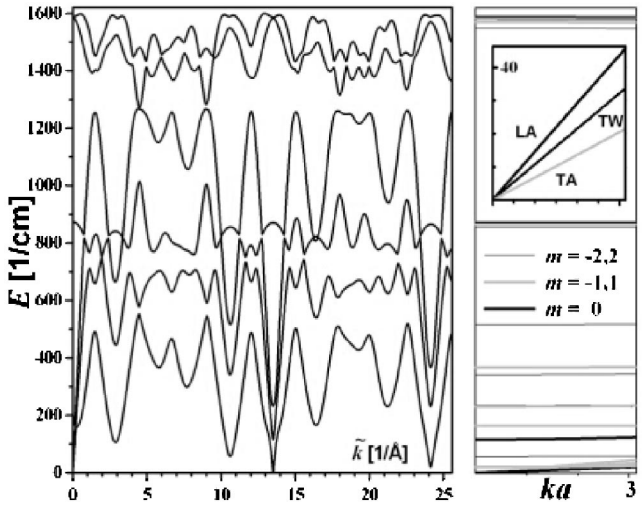

FIG. 1. Phonon dispersion curves for the (15,4) tube. Left panel: Bands assigned by the helical quantum numbers. Since $q=602$, $n=1$, and $a=74$ Å, the positive half of the helical BZ is $[0,25.6\ \text{Å}^{-1}]$, while $\tilde{m}=0$ for all bands; TA modes show up at $\tilde{k}=13.6\ \text{Å}^{-1}$, and LA and TW ones show up at $\tilde{k}=0$, in accordance with Eq. (8). Folding left panel to one 602th, one gets bands assigned by linear quantum numbers: $k\in[0,0.04\ \text{Å}^{-1}]$ and $m=-300,\ldots,301$. Right panel: In the linear BZ scheme the branches that in $k=0$ end up with the states listed in Table I together with the acoustic ones are presented. Note very small dispersion of all the bands. Also, the acoustic dispersion curves are given in the inset.

the latter are characterized by $m=1,\ldots,n-1$. In $k=0$, only the chiral tubes branches assigned by $m\neq 0,q/2$ remain double degenerate, while degeneracy is halved in other cases.[16,18]

Since m is related to the isogonal group (not a subgroup in the nonsymmorphic SWCNT's symmetry group), it is not conserved quantum number.[12,18] Particularly, it is not conserved in the Umklapp processes. Therefore, when the branches (and not only $k=0$ modes) are studied, it is advantageous to switch to the conserved, so-called helical quantum numbers $\tilde{k}$ and $\tilde{m}$ of the helical and the angular momenta. The range $(-q\pi/na,q\pi/na]$ of $\tilde{k}$, i.e., the helical BZ includes q/n Brillouin zones; on the contrary, the range of $\tilde{m}\in(-n/2,n/2]$ is q/n times smaller than that of m. Hence, a single band assigned by the helical $(\tilde{m}\tilde{k})$ quantum numbers splits into q/n bands in the linear (km) quantum numbers assignation. The order q of the principle axis of the isogonal group is usually very high, and the reduction of the number of branches by a factor q/n in the helical assignation at the cost of use of the q/n Brillouin zones may facilitate the visualization and interpretation of the branch structure.[13] Nevertheless, the two sets of quantum numbers are biuniquely related:

$$\tilde{k}=k+m\frac{2r\pi}{na}+\tilde{\kappa}\frac{2q\pi}{na},\quad \tilde{m}=m \bmod n, \tag{8}$$

$$k=\tilde{k}-\tilde{m}\frac{2r\pi}{na}+\kappa\frac{2\pi}{a},\quad m=(\tilde{m}-\kappa p)\bmod q. \tag{9}$$

Here the integers $\tilde{\kappa}$ and κ are introduced to provide $\tilde{k}\in(-q\pi/na,q\pi/na]$ and $k\in(-\pi/a,\pi/a]$, respectively. In Fig. 1 (left panel) we give the phonon dispersions for the (15,4) tube in the helical BZ scheme. As $n=1$, all the bands are labeled by zero helical angular momentum quantum number (no pure rotations!). Also, according to the relation (8) LA and TW modes carry zero helical momentum quantum number, while TA modes are characterized by nonvanishing $\tilde{k}$.

Concerning the obtained results, we stress out that the calculations are performed on the same 1280 tubes as before. The acoustic branches are obtained exactly: in the chiral tubes the transversal acoustic (TA) branches (beginning at $k=0$ with the double degenerate TA mode) are assigned by ${}_kE_1$ and ${}_kE_{-1}$ representations, the longitudinal acoustic (LA) and twisting acoustic (TW) branches by ${}_kE_0$, both of them being double degenerate over the positive half of BZ; in the achiral tubes, mirror planes cause additional degeneracy of the single fourfold TA branch assigned by the representation ${}_kG_1$, while the double degenerate LA and TW branches are assigned by ${}_kE_0^A$ and ${}_kE_0^B$ (differing by the vertical mirror parity), respectively. All the acoustic branches near the Γ point are linear in k, with the slopes, i.e., the sound velocities, being basically tube independent: $v_{\mathrm{TA}}=9.41$ km/s, $v_{\mathrm{LA}}=20.37$ km/s, $v_{\mathrm{TW}}=14.98$ km/s. These results agree with the previously reported ones,[3,4]despite some arguments on the quadratic k dependence of TA branch.[23,24] Acoustic dispersions of the (15,4) tube we give in the inset of the right panel of Fig. 1.

B. Specific heat

Theoretical predictions of the specific heat of some particular isolated SWCNT (Refs. 23,25) are in a reasonably good agreement with the heat capacity measurements of bundles of SWCNT's.[26–28] On the other side, up to our knowledge, the fine dependence of this quantity on the nanotube parameters has not been systematically studied. In this work we also calculate the specific heat for 225 isolated SWCNT's of all the chiralities and a wide range of diameters.

Close to $k=0$ the SWCNT acoustic branch we find to be linear in k. As this point is relevant in the specific heat context, we interrelate the graphene and SWCNT's acoustic branches. As it can easily be seen, the graphene TA mode turns into the tube's RBM upon rolling up the sheet into the cylinder. Similarly, the degenerated in-plane translations correspond to the TW and LA acoustic modes of a SWCNT if the translational directions are taken so to be parallel and orthogonal relative to the chiral vector. Finally, note that the (degenerate) SWCNT's TA modes are not related even to the graphene BZ Γ point, but to the certain edge point along the KM direction.

Close to the Γ point TA graphene acoustic branch is quadratical, while the other two (degenerate) subbands are linear in the wave vector. The van Hove singularity at the RBM frequency for all the SWCNT types and diameters means that the corresponding band is quadratic in k in $k=0$ vicinity. Further, in the zone folding method, the graphene bands TA

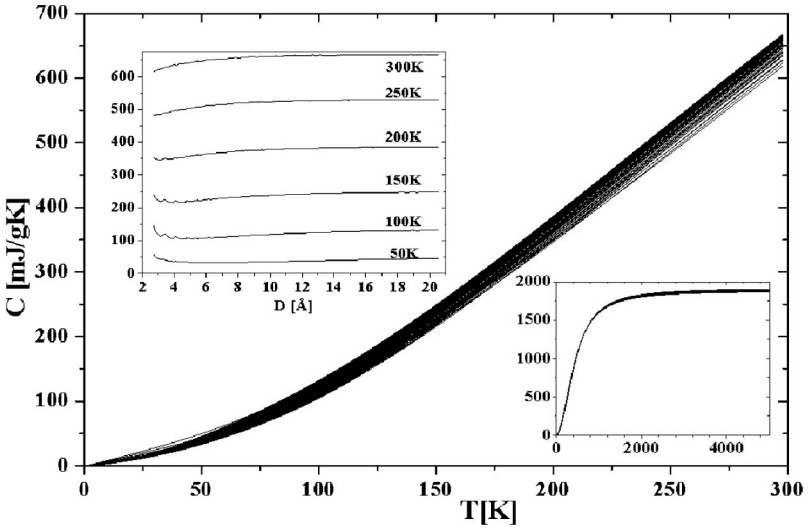

FIG. 2. The heat capacity C_{ph} dependence on temperature (upper panel) for 225 tubes, where diameters D range from 2.8 Å to 20.5 Å, i.e., starting with (2,2) and ending up at (24,4). The thickness of the curve we interpret by means of the upper inset, which illustrates, at various fixed temperatures, rather slow variation of the specific heat C_{ph} with the tube diameter. High-temperature limit can be seen from the lower inset.

are sliced in the direction described by chiral vector discretely, in the steps corresponding to the quantum number m. Thus, for sufficiently dense set of m values, the ''branches-along-m'' with fixed $k=0$ can be considered. Naturally, for TA branch (i.e., the one that matches the RBM) such m bands should be quadratic. We verified this on the chiral tube (53,18) having 49 044 bands: the series of ${}_0E_m$ bands that for $m=0$ gives RBM is quadratic in m near $m=0$. Among the acoustic modes, only the twisting mode m branch is quadratic in $m=0$.

Further it is relevant to determine precisely the temperature region in which only the acoustic modes contribute to the SWCNT specific heat. The phonon branch which corresponds to the minimal optical frequency is assigned as ${}_kE_2$ for chiral, and ${}_kG_2$ for achiral tubes, starting at $k=0$ with the Raman active ${}_0E_2$ and ${}_0E_2^+$ modes (see Table I). If $\omega_{\mathrm{min}}^{\mathrm{o}}$ is the frequency of the lowest-energy optical mode, then for the temperatures below $T_{\mathrm{o}} \approx \hbar\omega_{\mathrm{min}}^{\mathrm{o}}/6k_B$ the specific heat is determined by the acoustic phonon branches only.[23,26] We find its dependence on the tube diameter: $T_{\mathrm{o}}=(7.2+0.05D+1.045D^2)^{-1}10^3$ K (D in Å). The minimum $\omega_{\mathrm{min}}^{\mathrm{o}}$ is at k_{o}, which besides being chirality dependent (e.g., for achiral tubes $k_{\mathrm{o}}=0$) rapidly decreases with the tube diameter. Together with the above discussion on the RBM mode, this shows that the different regimes of the specific heat C_{ph} behavior are diameter dependent and that the crossover to the graphene T^2 dependence is continuously reached by the linear regime narrowing with the tube diameter.

In Fig. 2 the calculated specific heat temperature dependence up to 300 K is presented. It matches nicely the measured values.[27] The increase of the curve width with the temperature indicates that slight differences of C_{ph} between the tubes at higher temperatures are to be expected. The specific heat C_{ph} of a SWCNT shows the diameter dependence. Yet, as it is enlightened in the upper inset, the dependence on the diameter is saturated for considerably large tubes. In the lower inset of Fig. 2 we give the high-temperature limit that agrees reasonably well with the expected value $3k_B/m$ for the carbon systems.

The chirality shows no signature in the tubes specific heat. This is illustrated in Fig. 3 where the specific heat temperature dependence coincide for the tubes (10,10), (12,8), (15,4) and (11,9) with the same diameter $D=13.6$ Å but different wrapping angle. Besides, the log-log plot up to 100 K, the specific heat low- and high- temperature dependence, up to $T_{\mathrm{o}}(13.6\ \text{Å})=5$ K and 300 K are depicted in the inserted panels.

C. Overbending

As it is well known, in contrast to almost all covalent solids, graphite phonon branch that corresponds to the longitudinal high-energy optic mode has a local minimum at the Γ point. The feature is usually referred as ''overbending,'' since the local maxima thus appear at some general points of the BZ around the Γ point. According to our calculations the overbending pertains to the SWCNT's as well. As the overbending seems to be essential for exact theoretical interpretation of the laser excitation energy dependence and double-peak structure of the high-energy mode ($\approx 1600\ \mathrm{cm}^{-1}$) in first-order Raman spectra,[29] we analyze its characteristics

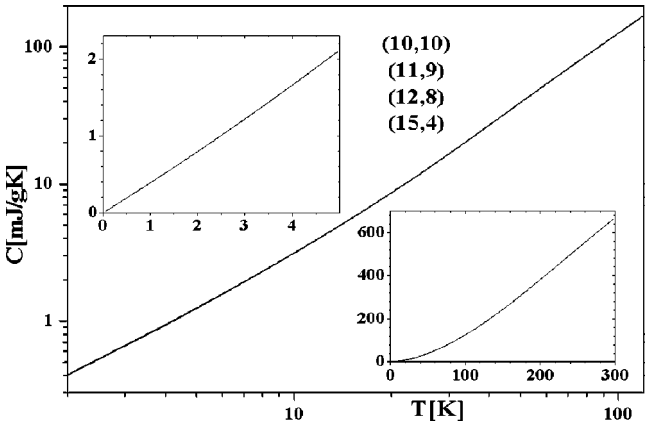

FIG. 3. The heat capacity C_{ph} for the four SWCNT's of the same diameter $D=13.6$ Å. In all the temperature regions their capacities coincide. Near $T=0$ (upper panel) capacity is linear in T.

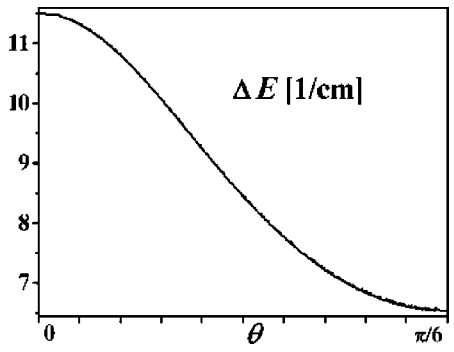

FIG. 4. The overbending ΔE as a function of the chiral angle θ for the 754 SWCNT's (among those with 2.8 Å$\leqslant D \leqslant$50.0 Å, the tubes with maximal D for given θ are chosen).

thoroughly, namely, these Raman spectra features have been quite recently attributed to the double-resonant process coming from the phonon modes close to the Γ point. Since the dispersion around $k=0$ is generally quite weak, the excitation energy dependence is expected to be very sensitive to the vibrational spectra details. In particular, the accurate theoretical investigation when related to the experiment may help the SWCNT's sample characterization. On the one side, from the Raman scattering measurements the slope of the excitation energy dependence of the high-energy mode frequency can be obtained. On the other side, the quantum theory of the double resonant Raman processes (which is, however, beyond the scope of this paper) relates this dependence to the overbending position k_0, its absolute value ΔE, its slope and the phonon eigenvectors (all of which can be easily calculated for any required spectrum of the SWCNT's diameters and chiralities).

The phonon branch exhibiting the overbending is assigned by $\tilde{m}=0$ quantum number for all the tubes. The corresponding irreducible representations[16] are $\tilde{k}E_0$ for $\mathcal{C}$, $\tilde{k}E_0^A$ for $\mathcal{Z}$, and $\tilde{k}E_0^B$ for $\mathcal{A}$ tubes. The displacement of the atom C_{000} as the function of $\tilde{k}$ is presented in Fig. 5. Again, the Bloch-like mode displacements of the other sites are given by Eq. (1).

We find the overbending $\Delta E=E(k_0)-E(0)$ (the energy difference of the phonon branch local minimum at $k=0$ and maximum at a nonvanishing k_0) to be strongly helicity dependent. On the other side, for a fixed chiral angle, it decreases with the diameter but rapidly saturates yet for the very thin tubes, hence showing no further diameter dependence whatsoever. In Fig. 4 the overbending ΔE as a function of the chiral angle θ is presented for the tubes that fall into the diameter dependence saturation region. The function is well fitted by

$$\Delta E(\theta) = -1.158 + \frac{9.57}{1-0.245\cos 6\theta}[\mathrm{cm}^{-1}].$$

Hence, the maximal overbending (11.5 cm^{-1}) is exhibited by the zig-zag and the minimal (6.50 cm^{-1}) by the armchair tubes. Further, we find that the local maximum appears for band $\tilde{m}=0$ at $\tilde{k}_0=-0.018+0.518/(1-0.143\cos 6\theta)$ [$\mathrm{Å}^{-1}$]; the D dependence rapidly saturates, and only for very small tubes' deviations from the above result appear (less than 1.5% of the helical BZ). By applying Eq. (8) one easily finds the corresponding k_0 and m_0 values. Only for the achiral tubes the overbending occurs in the $m=0$ band, while for the other tubes m increases with the diameter in steps of n along the ray $n(n_1,n_2)$. In the zig-zag $(n,0)$ tubes these bands start at $k=0$ by the mode assigned as ${}_0A_0^+$ without tangential component. In the armchair tubes, the $k=0$ mode of the band is assigned by ${}_0B_0^-$, and must be purely longitudinal. Then, the horizontal component of the displacements arises along the BZ, as presented in Fig. 5; the minimum of z displacement corresponds to the maximum of the band. Precise data on these quantities are needed for thorough quantum theoretical modeling of the double resonant high-energy Raman mode,[29] which might be useful for SWCNT's characterization.

V. SUMMARY

We have calculated the phonon dispersions and atomic displacements for achiral and chiral SWCNT's within the symmetry-based force-constant approach. The calculations

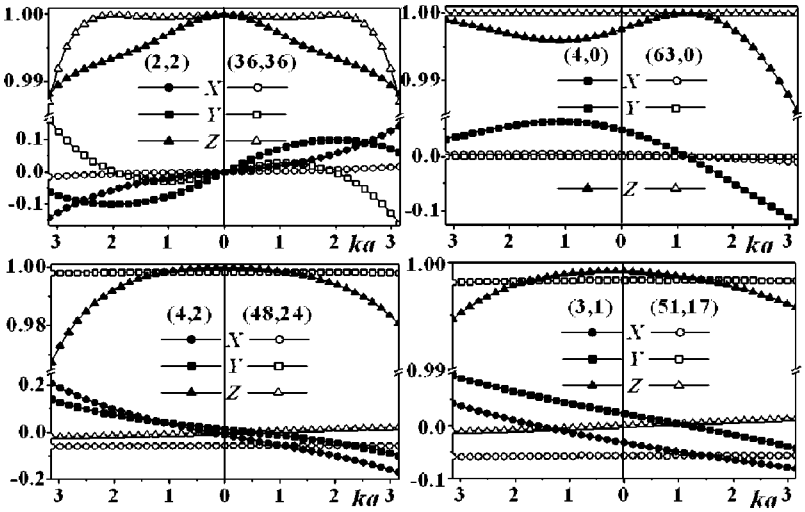

FIG. 5. The overbending displacement coordinates of the atom C_{000} for the allowed values $[0,\pi/a]$ of k. Displacements for all the other atoms may easily be found by use of Eq. (1). Left and right: two degenerate modes.

are of high precision, but still extremely efficient due to the complete incorporation of the symmetry. Besides the automatic assignment by the symmetry-based quantum numbers, the symmetry enables to express the normal mode displacements of the atoms along the tube, in the form of a Bloch-like wave (1), determined by the normal mode transformation law (irreducible representation) and the displacement of a single atom. In particular, this approach gives the exact solution to the twisting mode.

Extensive calculations have included sample of 1280 tubes, i.e., all SWCNT's with the diameters between 2.8 Å and 50.0 Å. The exhaustive data enabled to find the functional dependence of the frequencies of the Raman and IR active modes on the chiral angle and diameter, as well as determining the corresponding eigenvectors for all of them. As the IR and Raman active phonons are characterized by $k=0$, their classification is performed according to the isogonal symmetry group, i.e., $\boldsymbol{D}_q$ in the chiral and $\boldsymbol{D}_{2nh}$ in the achiral cases. As only the later contains the space inversion, for the chiral tubes there are simultaneously the IR and Raman active modes. Also, the antisymmetric Raman tensor components are found, for their expected significance in the resonant scattering. Finally, it is stressed out that under the light polarized linearly along the tube axis the armchair tubes are IR inactive.

The calculated phonon dispersions data we have also used to address the laser excitation energy dependence of the high-energy Raman active mode and have found the functional dependence of the overbending and of the wave vector at which the slope of the frequency shift changes the sign. If the proposed double resonant model for the high-energy Raman mode proves to be true, our results can be useful for the SWCNT's sample characterization. Finally, we have found the SWCNT's specific heat temperature (up to 4000 K) and diameter (at fixed temperatures) dependence and have determined the temperature T_o (as a function of the tube diameter) below which the population of the optical branches can be neglected when estimating the SWCNT specific heat.

ACKNOWLEDGMENTS

We appreciate discussions with C. Thomsen, S. Reich, and J. Maultzsch.

*Electronic address: edib@ff.bg.ac.yu; http://www.ff.co.yu/nanoscience

[1] A. Thess, R. Lee, P. Nikolaev, H. Dai, P. Petit, J. Robert, C.H. Xu, Y.H. Lee, S.G. Kim, A.G. Rinzler, D.T. Colbert, G.E. Scuseria, D. Tomanek, J.E. Fischer, and R.E. Smally, Science **273**, 483 (1996).

[2] M.S. Dresselhaus and P.C. Eklund, Adv. Phys. **49**, 705 (2000).

[3] R.A. Jishi, L. Venkataraman, M.S. Dresselhaus, and G. Dresselhaus, Chem. Phys. Lett. **209**, 77 (1993).

[4] R. Saito, T. Takeya, T. Kimura, G. Dresselhaus, and M.S. Dresselhaus, Phys. Rev. B **57**, 4145 (1998).

[5] E. Hernández, C. Goze, P. Bernier, and A. Rubio, Phys. Rev. Lett. **80**, 4502 (1998).

[6] J. Yu, R.K. Kalia, and P. Vashista, J. Chem. Phys. **103**, 6697 (1995); M. Menon, E. Richter, and K.R. Subbaswamy, *ibid.* **104**, 5875 (1996).

[7] J.P. Lu, Phys. Rev. Lett. **79**, 1297 (1997).

[8] V.N. Popov, V.E. Van Doren, M. Balkanski, Phys. Rev. B **59**, 8355 (1999); **61**, 3078 (2000).

[9] D.H. Robertson, D.W. Brenner, and J.W. Mintmire, Phys. Rev. B **45**, 12 592 (1992).

[10] D. Sánchez-Portal, E. Artacho, J.M. Soler, A. Rubio, and P. Ordejón, Phys. Rev. B **59**, 12 678 (1999).

[11] O. Dubay and G. Kresse, Phys. Rev. B **67**, 035401 (2003).

[12] M. Damnjanović, I. Milošević, T. Vuković, and R. Sredanović, Phys. Rev. B **60**, 2728 (1999).

[13] J. Maultzsch, S. Reich, C. Thomsen, E. Dobardžić, I. Milošević, and M. Damnjanović, Solid State Commun. **121**, 471 (2002).

[14] I. Milošević and M. Damnjanović, Phys. Rev. B **47**, 7805 (1993).

[15] M. Damnjanović and I. Milošević, J. Phys. A **28**, 1669 (1995).

[16] M. Damnjanović, T. Vuković, and I. Milošević, J. Phys. A **33**, 6561 (2000).

[17] I. Milošević, A. Damjanović, and M. Damnjanović, *Quantum Mechanical Simulation Methods in Studying Biological Systems*, edited by D. Bicout and M. Field (Springer-Verlag, Berlin, 1996), Chap. XIV.

[18] T. Vuković, I. Milošević, and M. Damnjanović, Phys. Rev. B **65**, 045418 (2002).

[19] M. Born and K. Huang, *Dynamical Theory of Crystal Lattices* (Oxford University Press, Oxford, 1954).

[20] O. Madelung, *Solid State Theory* (Springer-Verlag, Berlin, 1978).

[21] D.A. Long, *Raman Spectroscopy* (McGraw-Hill, New York, 1977).

[22] O.E. Alon, Phys. Rev. B **63**, 201403 (2001). The irreducible representations A_1, A_2, E_1 and E_2 in this paper correspond to ours ${}_0A_0^+$, ${}_0A_0^-$, ${}_0E_1$ and ${}_0E_2$ for chiral tubes, while for the achiral ones A_{1g}, A_{2u}, E_{1u}, E_{1g} and E_{2g} correspond to ${}_0A_0^+$, ${}_0A_0^-$, ${}_0E_1^+$, ${}_0E_1^-$ and ${}_0E_2^+$.

[23] V.N. Popov, Phys. Rev. B **66**, 153408 (2002).

[24] G.D. Mahan, Phys. Rev. B **65**, 235402 (2002).

[25] L.X. Benedict, S.G. Louie, and M.L. Kohen, Solid State Commun. **100**, 177 (1996); A. Charlier, E. McRae, M.-F. Charlier, A. Spire, and S. Forster, Phys. Rev. B **57**, 6689 (1998).

[26] A. Mizel, L.X. Benedict, M.L. Cohen, S.G. Louie, A. Zettl, N.K. Budraa, and W.P. Beyermann, Phys. Rev. B **60**, 3264 (1999).

[27] J. Hone, B. Batlogg, Z. Benes, A.T. Johnson, and J.E. Fischer, Science **289**, 1730 (2000).

[28] J.C. Lasjaunias, K. Biljaković, Z. Benes, J.E. Fischer, and P. Monceau, Phys. Rev. B **65**, 113409 (2002).

[29] J. Maultzsch, S. Reich, and C. Thomsen, Phys. Rev. B **65**, 233402 (2002).